Original Article

Direct ESI-MS of Ionic Liquids Using High-Pressure Electrospray From Large-Bore Emitters Made of Micropipette Tips

Takeshi Matsuda and Lee Chuin Chen[*]

Faculty of Engineering, University of Yamanashi, Yamanashi, Japan

Electrospray ionization mass spectrometry of neat undiluted ionic liquid (IL) and the analysis of protein with the doping of IL were performed using high-pressure electrospray. The use of disposable micropipette tips as emitters eased the handling of viscous and easy-to-clog samples and improved the reproducibility of the measurement. A high-pressure operation enabled the stable electrospray of the highly conductive IL from these relatively large bore emitters. The measurement of the current–voltage relationship of 1-ethyl-3-methylimidazolium tetrafluoroborate (Emim BF_4) revealed an unusual negative differential resistance that has not been seen in the typical atmospheric or high-pressure electrospray. Mass spectrometric analysis of this IL also showed the characteristic response of various ion species with the emitter voltage. When added to the commonly used protein solution, the mass spectrum also showed protein peaks that correspond to the adduction of fluoroboric acid molecules (HBF_4).

1. INTRODUCTION

An ionic liquid (IL) is a molten salt in the liquid state at room temperature. As the liquid consists entirely of ions, the coulombic interaction between them is so strong that the vapor pressure of IL is practically zero. Its surface tension is lower than water and the viscosity varies over a wide range of values depending on the chemical composition. It is electrically conductive, and thermally stable and has found various applications in the field of electrochemistry, batteries, extraction, *etc*. Hydrophilic ILs such as 1-butyl-3-methylimidazolium chloride are also known to dissolve cellulose.[1] The application of ILs also includes propulsion in the space program. The negligible vapor pressure and the high electrical conductivity make IL a suitable choice for the propellent in the electrospray-based propulsion system.[2] Similar to aqueous/organic solution, the electrospray of IL can be formed by applying a high potential difference between IL and the counter electrode. At low flow rates, the molecular ions of ILs have been reported to sustain operation in the pure ion evaporation regime.[2] Instead of a single emitter, the IL thruster has also been designed to contain a 2-dimensional array of electrospray emitters to increase the thrust per unit area.[3] Ionic propulsion based on heated electrospray of IL under the pure ionic regime also exists.[4] The characterization of electrospray of IL has been performed in a vacuum by feeding IL to the emitter capillary,[5] and by wetting a sharp tungsten needle with IL.[6] Both studies indicated that the electrospray of IL in a high vacuum generates an emission consisting of ions and charged droplets.

In the area of mass spectrometry, ILs have also been used for the desorption/ionization taking place in the high vacuum. For example, ILs derived from α-cyano-4-hydroxycinnamic acid were reported to be suitable matrices for secondary ion mass spectrometry (SIMS) to enhance the ion signal.[7] IL-based laser absorbing matrices for matrix-assisted laser desorption/ionization (MALDI) were also reported.[8,9] An advantage of the IL matrix over the solid one is the homogeneity of the sample which improves the shot–shot reproducibility and eliminates the need to search for the sweet spot. In the case of electrospray ionization mass spectrometry (ESI-MS), the addition of IL into hydrocarbon solvents such as hexane and toluene was found to enable the electrospray and the ionization of the dissolved analytes in those non-polar solvents.[10] IL has also been used to produce cluster ion beams for SIMS.[11] A target current greater than 200 nA was reported using the electrospray of IL at 50 nL/min. The generation of the IL ion beam was also performed from a tungsten needle.[12] Similar to the normal electrospray, the effect of electrochemical reactions of IL was also observed.[13]

As for the MS analysis of ILs, it has been performed by MALDI,[14] liquid injection field desorption/ionization MS (FD/I-MS),[15] high-pressure FD,[16] atmospheric pressure FD,[17] desorption from sharp needles of cactus,[18] and

*Correspondence to: Lee Chuin Chen, *Faculty of Engineering, University of Yamanashi, 4–3–11, Takeda, Kofu, Yamanashi 400–8511, Japan*, e-mail: leechuin@yamanashi.ac.jp
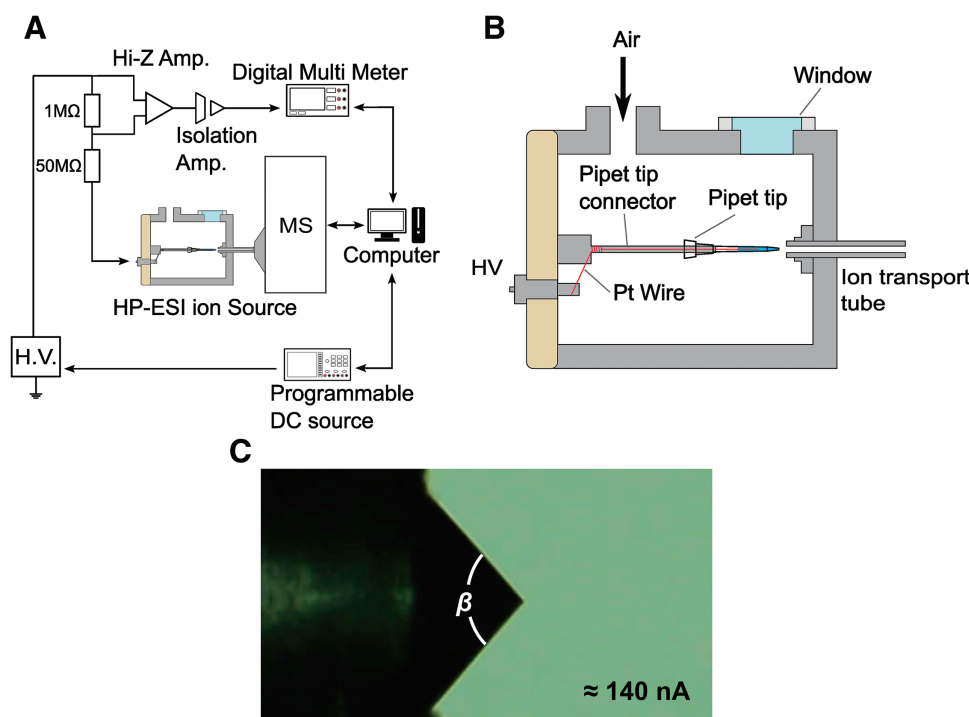
Fig. 1. (A) Schematic diagram of the high-pressure ESI source and the electrical configuration for the measurement of spray current and the feedback system. A computer-based feedback system was used to control the HV supply for constant current operation. (B) Inside the high-pressure ESI ion source. (C) Taylor cone of the IL (Emim BF$_4$). The spray current value is 140 nA in (C), and β is the apex angle of the Taylor cone. ESI, electrospray ionization; Emim BF$_4$, 1-ethyl-3-methylimidazolium tetrafluoroborate; IL, ionic liquid.

ESI.[19–21] The electrospray of IL diluted in water and organic solvent can be done using a conventional ESI source.[19] Electrospray of undilute neat IL has been performed using a normal electrospray emitter,[20] but a heated curtain gas was important to observe ion signal. The heating effect was speculated to reduce the viscosity of the IL in the ESI capillary.[20] In another arrangement, the droplet IL was anchored to the tip of a stainless-steel wire that was placed in the path of a moving desolvation gas toward the MS inlet.[21]

Here, we investigate the emission of droplets/ions from the highly stable Taylor cone of the undiluted IL directly from a micropipette tip with an inner diameter of 0.4 mm. The ion source here utilizes the concept of high pressure, an ESI stabilizing technique that has been developed previously to handle the liquid with high surface tension such as pure aqueous solution.[22–24] In the sealed chamber, the pressure of the gas surrounding the ESI emitter and the counter electrode was increased beyond 1 atm to reduce the mean free path of electrons as a means to increase the onset voltage for gaseous breakdown. The threshold for electrospray was, however, unaffected by the gas pressure. The increased insulation under high pressure enables the generation of nano-ESI from a micropipette tip with a large inner diameter (>100 µm) in the conventional sense.[25] With the precision modulation of the emitter voltage, the flow rate can be finely tuned to investigate the ionization response,[26] and other phenomena such as field-induced oxidation that is related to the size of the nanodroplets.[27]

2. EXPERIMENTAL SECTION

2.1 Ion source and mass spectrometer

Figure 1A shows the block diagram for the configuration of the experiment which consisted of a high-pressure electrospray ion source, a commercial mass spectrometer, and a computer-based feedback control system. The ion source (Fig. 1B) was pressurized to 0.5 MPa gauge pressure (~6 atm) with dry air (relative humidity <10%) using an air compressor. A micropipette tip (epT.I.P.S., 0.5–20 µL, Eppendorf, Hamburg, Germany) with an inner diameter of 0.4 mm was used as the emitter. The high voltage was applied to the solution *via* a platinum wire (Diameter: 0.2 mm, Nilaco, Tokyo, Japan) inserted into the micropipette tip. The ion source was connected directly to a commercial mass spectrometer (Exactive, Thermo Fisher Scientific, Waltham, US) *via* a custom-made ion transport tube with an inner diameter of 0.25 mm. The pressure in the first pumping stage of the mass spectrometer was about 1 mbar. The spray current was detected by sensing the voltage drop across a 1 MΩ resistor using a high-impedance amplifier (INA 116, Texas Instruments, Dallas, US). The amplified and isolated signal was read using a digital multimeter and the reading was recorded by a personal computer. When operated under a constant current mode, the deviation of the measured current from a preset target current was used as the error signal to perform feedback correction to the emitter voltage.[28] The instrument settings for the mass spectrometer were as follows: the ion transport tube temperature was 200°C–300°C, the voltages of the inlet capillary and the tube lens were 60 V, and the skimmer voltage was 20 V.

2.2 Sample preparation

The IL used in this study was 1-ethyl-3-methylimidazolium tetrafluoroborate (Emim BF$_4$, Product Number: E0496) purchased from the Tokyo Chemical Industry (Tokyo, Japan). The electrical conductivity measured using a conductivity meter (Mettler Toledo SevenExcellence, Greifensee, Switzerland) was approximately 1.8 S/m. Bovine heart
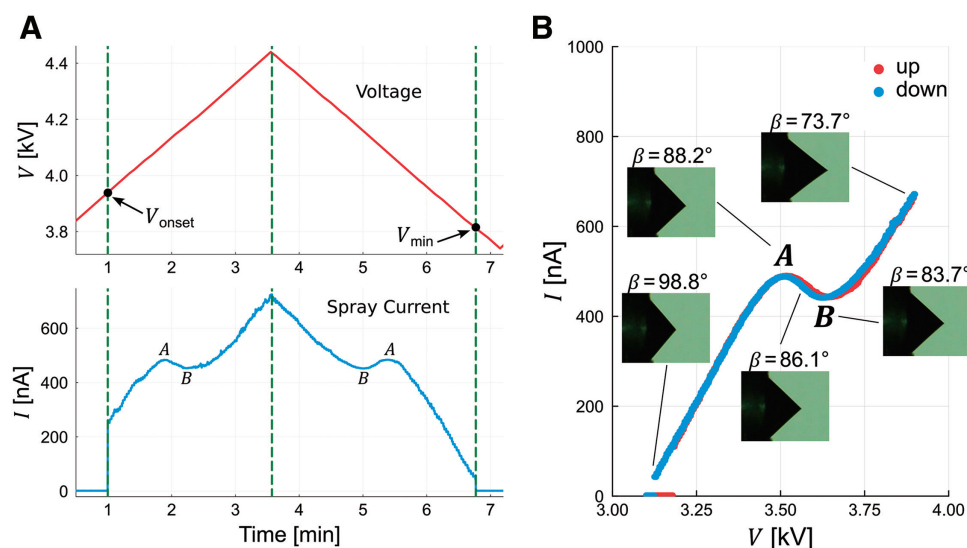
Fig. 2.   (A) Measurement of spray current by scanning the emitter voltage up and down. (B) The Constructed current–voltage (I–V) curve. Insets show the images of the Taylor cone acquired at different voltages.

cytochrome c was purchased from Wako (Osaka, Japan) (Product Number: 033-16821). Ammonium acetate was purchased from Kanto Chemical (Tokyo, Japan) (Cat. No. 01969-23). Pure water used for solution preparation was purified using Simplicity UV (Millipore, Bedford, MA, USA).

3.   RESULTS AND DISCUSSION

3.1   Taylor cone, I–V, and I–Q characteristics

Figure 1C shows the formation of a highly stable Taylor cone of IL anchored at the distal end of the micropipette tip. The inner diameter of the tip, which was also the base diameter of the Taylor cone, was ~0.4 mm. This value was relatively large compared to the standard ESI emitters. To initiate a stable Taylor cone and spray current, a high pressure of greater than 3 atm was needed to prevent the gaseous breakdown that induced a large flow of electric discharge current. Interestingly, when the Taylor cone was established, the pressure of the ion source could be reduced to ~1.2 atm without triggering significant electrical discharge. Nevertheless, accidental ejection of a large amount of IL could cause contamination to the ion inlet and the tube lens. Thus, for the ease of the experiment and to ensure the reproducibility of measurements, the pressure of the ion source was maintained at ~6 atm (0.5 MPa gauge pressure). The apex angle of the Taylor cone was denoted as β in Fig. 1C. The theoretical value of β for a truly static Taylor cone was 98.6°.[29] The apex angle in practice, however, was found to change with the applied voltage.

Figure 2A shows the change in measured spray current during the voltage scanning process. To measure the current–voltage relationship, the voltage applied to the IL was slowly increased in a stepwise manner using a computer-controlled system. Upon reaching a preset maximum value, the voltage was decreased to a preset minimum value (see the triangular scanning pattern in Fig. 2A). The sweeping of voltage was performed at the highest resolution of 0.5 V/step. The step interval was approximately 0.15 s. Overall, the ramping rate was approximately 3.3 V/s. A ramping rate of a few V/s ensured that the sweeping was slow enough not to excite the liquid oscillation. The result in Fig. 2A shows that an onset

voltage (V_{onset}) was required to turn the originally spheroidal meniscus into a conic meniscus (Taylor cone). Once the conic meniscus was established, it could be sustained at a voltage lower than the onset voltage down to a minimum value at V_{min}. The lowest flow rate and current were obtained at V_{min} at which the meniscus has an apex angle very close to the theoretical Taylor cone apex angle. This result was consistent with our previous work on aqueous Taylor cone.[25–27]

The measured current and voltage were used to construct the current–voltage (I–V) curve for the IL shown in Fig. 2B. The data points corresponding to the voltage scanning up process are colored in red, whereas the data points obtained by scanning down voltage were colored in blue. Unlike the typical syringe pump-controlled electrospray operated at a constant flow rate, there was no hysteresis-like pattern,[28] that is, the rise and fall of spray current followed the same path, and the data points obtained by increasing and decreasing voltage overlapped nicely with each other. The insets show the conditions and the apex angle of the Taylor cone. Owing to the high electrical conductivity of the IL (~1.8 S/m) and the stable spraying condition provided by the high pressure, the stable cone jet mode could be operated to support a wide dynamic range of spray current from 50 to 900 nA. The measurement of higher currents was not performed due to the limitation of the measurement circuit and the risk of ion source contamination.

Overall, the I–V relationship was not linear, but there were two regions where the I–V was approximately linear. One was for the current range from 50 to ~450 nA, and another one was for ~450 to 700 nA. Interestingly, the I–V curve shows two stationary points (marked as A and B) at ~3.5 kV and ~3.6 kV. The locations of these two stationary points were easily reproduced either by increasing or decreasing the applied voltages. In the typical flow rate regulated electrospray, the stationary or "transition" point in the staircase I–V curve indicates the transition of spraying mode, that is, from pulsation to cone-jet or from cone jet to multi-jet modes.[28] Here, the I–V curve resembled a cubic function and has two stationary points labeled as A and B in Figs. 2A and 2B. When the voltage was lower than point A, and above point B, the spray current increased, as expected, with the voltage.
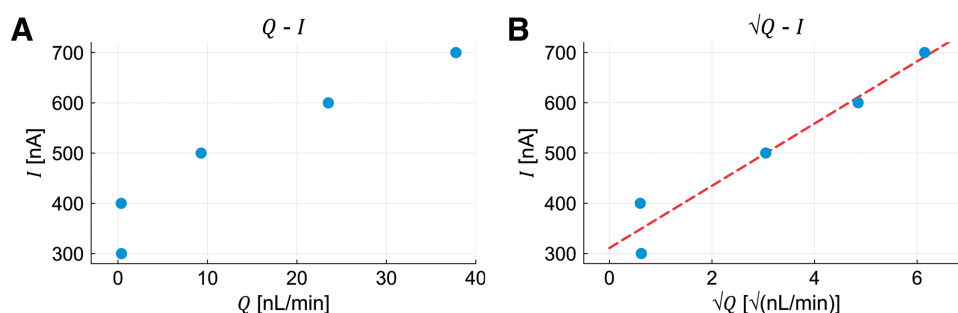
Fig. 3.   (A) The measurement of spray current I and the volumetric flow rate Q of the IL. (B) The plot of I versus $\sqrt{Q}$. IL, ionic liquid.

The peculiar trend was observed when the voltage was within the region of point A and point B in which the spray current, against the common intuition, decreased with the increase in voltage. As verified by the microscopic images, the transition points were not due to the change in spraying mode. Also, unlike the current, the apex angle of the Taylor cone decreased with the voltage without showing signs of transition points. At a surface element away from the jet, the apex angle was the result of the balancing between the surface tension and the normal electric stress. A smaller value of apex angle indicated a higher electric field at a higher voltage, an expected observation.

The region between A and B clearly exhibited a negative differential resistance. We speculated that the phenomenon might be related to the multiple components of electrospray current. The phenomenon of negative resistance exists in electronic devices such as tunnel diodes. In that case, the diode current consists of a nonlinear tunneling current in addition to the normal diode current. The tunneling effect was unrelated here, but there was a similarity to our experiment in that the measured electrospray current was the sum of the normal spray current and the current attributed to direct ion emission. Direct ion emission is known to exist in the electrospray of IL in vacuum.[2] Here, the current density for the direct ion emission ought to be higher at a lower voltage when the flow rate is low and the initial charged droplet is small. The direct emission current was expected to diminish when a higher flow rate was induced by a higher emitter voltage. When the voltage exceeded the value at point B, the current was believed to be dominated by the normal spray current. As the electrospray was performed under high pressure, the space charge effect caused by the cloud of emitted droplets and ions might also play a role to retard the charge emission from the Taylor cone's tip. The current would increase again when the space charge retardation was overcome by a further increase in voltage.

Figure 3A shows the measurement of flow rates at different spray currents. The flow rate was estimated by accurately measuring the mass of the loaded IL before and after spraying IL at a constant current. The volumetric flow rate was derived from the change in mass under a known spraying time. For the cone-jet mode with solutions of large conductivity, the following relationship between spray current and flow rate has been proposed.[30]

$$I_F = g\left(\epsilon_r\right)\left(\frac{\gamma K Q}{\epsilon_r}\right)^{1/2} \qquad (1)$$

where ϵ_r is the relative permittivity, γ is the surface tension, and K is the electrical conductivity of the liquid. Coefficient $g(\epsilon_r)$ was an experimentally determined constant. In addition, another model proposed the following relationship between spray current and flow rate for conductive liquid.[31]

$$I_G = 2.6\left(\gamma K Q\right)^{1/2} \qquad (2)$$

Both equations give a $I \propto \sqrt{Q}$ relationship to the spray current and flow rate. To verify this empirical power law, the square root of the flow rate was plotted against the spray current in Fig. 3B. The fitted linear regression line shows a reasonable proportional relationship existed between $I - \sqrt{Q}$ for $I \geq 500$ nA. The deviation in the low flow rate region (<10 nL/min) was believed due to the error in flow rate measurement. A higher value of current might be due to the contribution from direct ion emission.

3.2   Mass spectrum of Emim BF$_4$

Figure 4 shows the typical mass spectra of Emim BF$_4$ obtained by spraying the neat IL directly without dilution using the high-pressure ESI source. The molecular structure of Emim BF$_4$ is shown in Scheme 1. In the following discussion, the cation of Emim BF$_4$ is assigned as X$^+$, and the anion as Y$^-$. Figure 4A shows the mass spectrum in the low-mass region, and Fig. 4B is the medium to high-mass region. Overall, the cation X$^+$ and the cation-adducted neutral molecule of IL, that is, (XY)X$^+$ dominate the mass spectrum. The dominant peaks (labeled with red circles) with equal spacing of 198.1 in Fig. 4B are the clusters of the IL in the form of (XY)$_n$X$^+$, with n up 19. Their associated fragments in the form of $[(XY)_nX - C_3H_8]^+$, labeled as blue triangles, were also observed. In the high mass region (500–4000), (XY)$_4$X$^+$ was the highest peak, followed by (XY)$_7$X$^+$. As shown in the close-up mass spectrum for the m/z region of 500 to 1000, the intensity of (XY)$_2$X$^+$ was relatively low. For $n = 3$, the intensity of the fragment was higher than the precursor (XY)$_3$X$^+$. Fragments for the cation, (XY)X$^+$ and (XY)$_2$X$^+$ were not detected. The fragmentation could be due to the in-source dissociation of the ethyl and methyl groups of the IL during the transfer of ions.

3.3   Scanning voltage MS for IL

To evaluate the ion response of (XY)$_n$X$^+$ under different flow rates, the MS acquisition was performed by gradually increasing the emitter voltage until a preset maximum value, and then decreasing the voltage to the minimum value as shown in Fig. 5A. The recorded spray current is shown in Fig. 5B. The acquisition of mass spectra was started in sync
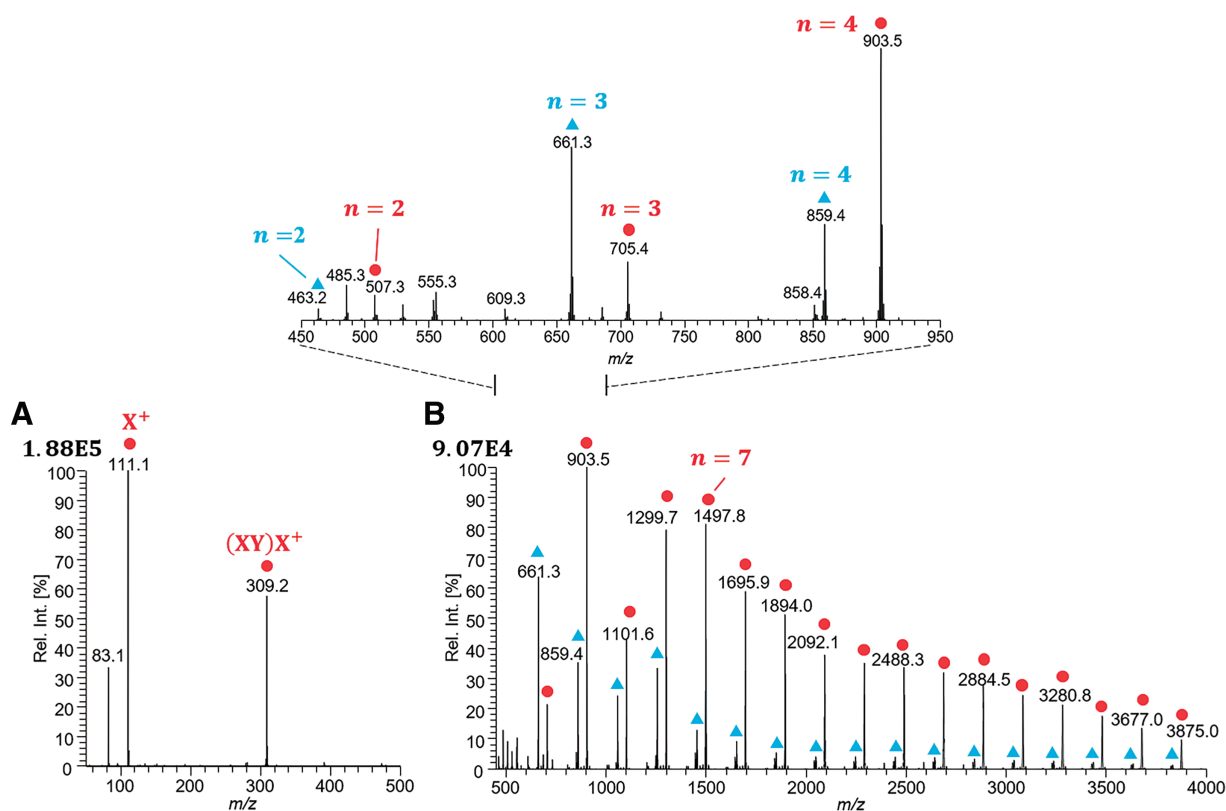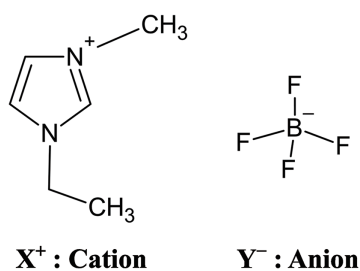
Fig. 4. Mass spectra acquired from the neat IL ([Emim][BF4]) using high-pressure ESI. (A) Mass spectrum in the low mass region. (B) Medium to high mass region. The inset shows the close-up mass spectrum for (B). Emim BF_4, 1-ethyl-3-methylimidazolium tetrafluoroborate; ESI, electrospray ionization; IL, ionic liquid.

Scheme 1. Structure of Emim BF_4.

with the scanning of voltage using the contact control of the mass spectrometer originally reserved for synchronizing the data acquisition with the liquid chromatography devices. The incremental and decremental rate was 0.5 V per step. Extracted ion chromatogram (EIC) of the selected ion signal for $(XY)X^+$, $(XY)_4X^+$, and $(XY)_{13}X^+$ are shown in Figs. 5C to 5E. Overall, all ion signals show an increasing trend with the decrease in spray current. However, the highest ion signal was reached at ~100 nA, which was slightly higher than the minimum spray current right before the collapse of the Taylor cone. For $(XY)X^+$, the ion signal showed another hump, that is, a local maximum at which the position coincided approximately with the transition point A of the spray current (~500 nA). Such hump was not observed with other larger clusters. Also, right after this point, the signal for higher-order clusters such as $(XY)_4X^+$ and $(XY)_{13}X^+$ started to show an appreciable increase in ion intensity in the direction of decreasing current. In sum, all IL-related ions were detected in most abundance when the current was near its minimum. This is conceivable as the generated droplets were nearly the smallest there was a

possibility of direct emission of cluster ions. As for the $(XY)X^+$ ion, its abundance showed an increasing trend with the voltage in the time duration of 5–6 min. The reason could be due to the increase in the sample introduction rate at a higher flow rate, and for this ion species, the release of ions from a relatively large droplet was still attainable compared to other species. A higher voltage in 3.5–5 min resulted in a further increase in flow rate and droplet size that reduced the ionization efficiency. The intensity of the fragment ions for $n > 2$ follows the trend of their intact ions. As for $(XY)X^+$, its fragment ion signal was too weak to be significant. The relationship between the generated ion species and the observed anomaly in the spray current will be further investigated in the future.

3.4 MS of protein with the addition of Emim BF_4

As described previously, IL-related ions could be generated with high intensity from the direct electrospray of IL. We have also attempted to generate macromolecules such as protein dissolved in the neat IL. But despite our best efforts, no protein signal was detected from the undiluted IL even with protein concentration up to >10^{-4} M. This prompted us to investigate to what extent should the IL be diluted to generate detectable protein ions. The measurement was performed using 8 μM cytochrome c in 100 mM ammonium acetate aqueous solution with the addition of Emim BF_4. The maximum tolerable concentration of IL to yield a reproducible ion signal for cytochrome c was found to be in the order of 10^{-3} M. At this concentration, the pattern of the MS and the ion intensity was dependent on the spray current (see Fig. 6). Clean mass spectra with the highest ion intensity were obtained at the lowest possible spray current. That condition corresponded to the generation of the smallest
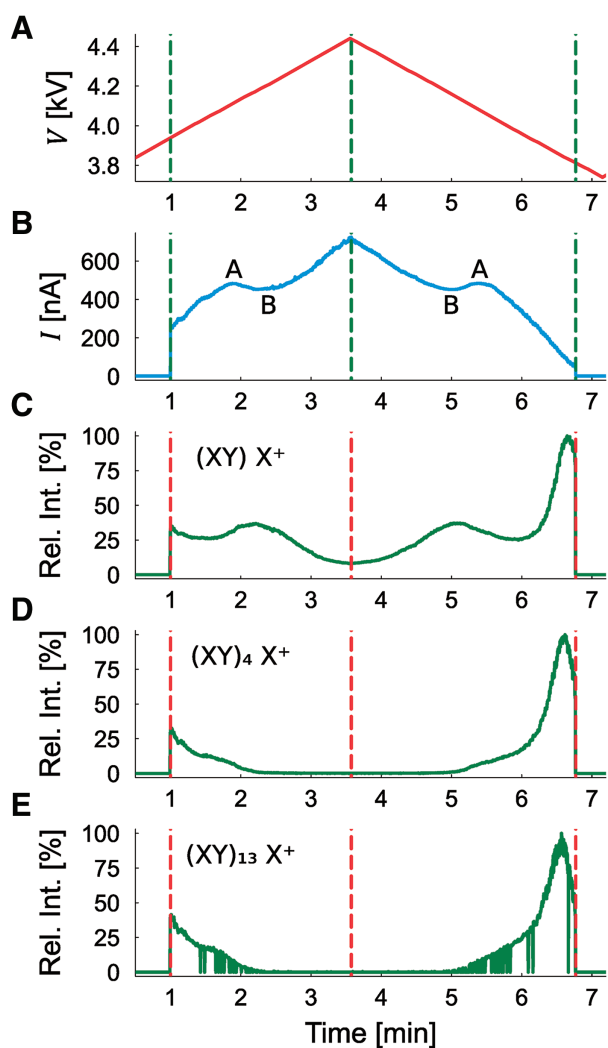
Fig. 5. (A) The ramping up and down of emitter voltage. (B) Measured spray current. (C) EIC for $(XY)X^+$, where X is the cation and Y is the anion of the IL. (D) EIC for $(XY)_4X^+$. (E) EIC for $(XY)_{13}X^+$. EIC, extracted ion chromatogram; IL, ionic liquid.

Fig. 6. Mass spectra of cytochrome c (8 μM) prepared in 100 mM ammonium acetate aqueous solution doped with 1 mM Emim BF$_4$. Spray currents are (A) 80 nA, (B) 200 nA, (C) 400 nA, (D) 600, and (E) 800 nA. Red asterisks in the insets denote the protonated, and blued asterisks denote the peak with adduction of HBF$_4$ for charge state 6+. Emim BF$_4$, 1-ethyl-3-methylimidazolium tetrafluoroborate.

liquid droplet.[25–27] The moderately charged ion species with the highest peak at 10+ dominated the mass spectrum. There was also a presence of low charge state species of 6+ and 7+. The presence of IL in the protein solution caused significant adduction of fluoroboric acid molecules (HBF$_4$) to the low-charge-state species of 6+ and 7+. Those ions were in the form $[M + aH + bHBF_4]^{a+}$. The highly charged and the low-charge-state ions (6+ and 7+) were believed to follow different ionization routes. The highly charged ions can accumulate near the surface of the precursor droplet and be ejected directly,[32] or transported to the secondary droplet *via* Rayleigh fission during the early stage of droplet evaporation. We speculate that the local concentration of anions surrounding protein during the formation of high-charge-state ions was lower than that of low-charge-state ions. The formation of native-like low-charge-state ions follows the route of the charge-residue model, that is, the excess charges were deposited on the molecule when the solvent was fully evaporated. Due to the non-evaporative nature of the IL, the concentration of the anion should be higher in the last-stage droplet that produces the gas phase ions.
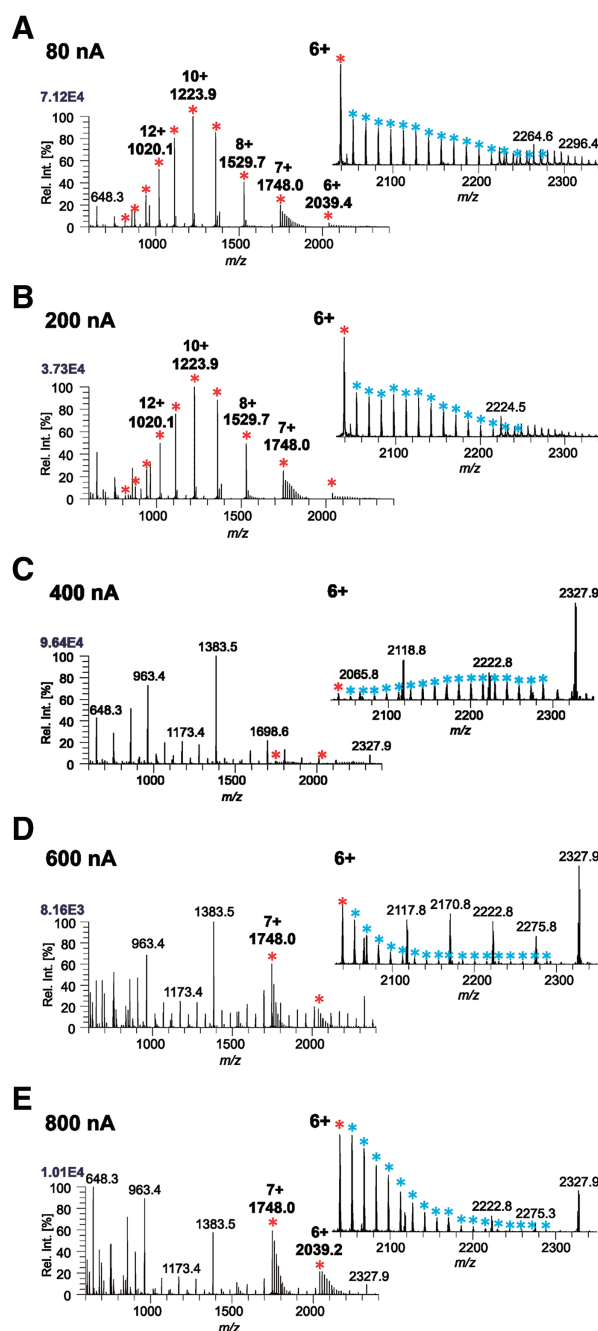
Although with low ion intensity, the largest observable number of neutral HBF$_4$ adducted to cytochrome c was 18 for the charge state 6+ and 17 for the charge state 7+. The cytochrome c here was from a bovine heart and the total number of basic sites (lysines, arginines, histidines, and N-termini) was 24. For the protonated species, the relationship between the charge state and the largest number and the maximum number of acid molecule adducts was known to be equal to the total number of basic sites.[33,34] Previous works used mineral acids such as HI[33] and

$HClO_4$.[34] Here, our result shows that the relationship was also true for the solution containing IL with large size anion such as BF_4^-.

4. CONCLUSION

The electrical and mass spectrometric characterization of a highly conductive IL has been performed. The formation of a highly stable Taylor cone was achieved using the high-pressure ESI technique where the liquid was electrified in an environment with gas pressure greater than atmospheric pressure. The spray current–voltage relationship showed the presence of two transition points even when the electrospray was in the cone-jet mode. The region between these transition points exhibited a negative differential resistance, a phenomenon that was not seen in the typical electrospray of common solvents and aqueous solution for atmospheric pressure or high-pressure electrospray. The finding warranted further investigation. The direct ESI-MS of the undiluted neat IL also showed the presence of IL-related cluster ions, in addition to the cation of IL (positive mode ion). The ion response under varying voltage also revealed a slightly different pattern for the cation-adducted single IL molecule as compared to other higher-order IL molecular clusters. For the aqueous protein solution containing ammonium acetate and Emim BF_4, the adduction of HBF_4 to the low-charge-state species of protein was also observed.

ACKNOWLEDGEMENTS

REFERENCES

1) R. P. Swatloski, S. K. Spear, J. D. Holbrey, R. D. Rogers. Dissolution of cellulose with ionic liquids. *J. Am. Chem. Soc.* 124: 4974–4975, 2002.

2) I. Romero-Sanz, R. Bocanegra, J. Fernandez de la Mora, M. Gamero-Castaño. Source of heavy molecular ions based on Taylor cones of ionic liquids operating in the pure ion evaporation regime. *J. Appl. Phys.* 94: 3599–3605, 2003.

3) B. Gassend, L. F. Velasquez-Garcia, A. I. Akinwande, M. Martinez-Sanchez. A microfabricated planar electrospray array ionic liquid ion source with integrated extractor. *J. Microelectromech. Syst.* 18: 679–694, 2009.

4) I. Romero-Sanz, I. Aguirre de Carcer, J. Fernandez de la Mora. Ionic propulsion based on heated Taylor cones of ionic liquids. *J. Propuls. Power* 21: 239–242, 2012.

5) M. Gamero-Castaño. Characterization of the electrosprays of 1-ethyl-3-methylimidazolium bis(trifluoromethylsulfonyl) imide in vacuum. *Phys. Fluids* 20: 032103, 2008.

6) Y.-H. Chiu, G. Gaeta, D. J. Levandier, R. A. Dressler, J. A. Boatz. Vacuum electrospray ionization study of the ionic liquid, [Emim][Im]. *Int. J. Mass Spectrom.* 265: 146–158, 2007.

7) J. J. D. Fitzgerald, P. Kunnath, A. V. Walker. Matrix-enhanced secondary ion mass spectrometry (ME SIMS) using room temperature ionic liquid matrices. *Anal. Chem.* 82: 4413–4419, 2010.

8) D. W. Armstrong, L.-K. Zhang, L. He, M. L. Gross. Ionic liquids as matrixes for matrix-assisted laser desorption/ionization mass spectrometry. *Anal. Chem.* 73: 3679–3686, 2001.

9) J. A. Crank, D. W. Armstrong. Towards a second generation of ionic liquid matrices (ILMs) for MALDI-MS of peptides, proteins, and carbohydrates. *J. Am. Soc. Mass Spectrom.* 20: 1790–1800, 2009.

10) M. A. Henderson, J. S. McIndoe. Ionic liquids enable electrospray ionisation mass spectrometry in hexane. *Chem. Commun.* 2006: 2872–2874, 2006.

11) Y. Fujiwara, N. Saito, H. Nonaka, T. Nakanaga, S. Ichimura. Characteristics of a charged-droplet beam generated by vacuum electrospray of an ionic liquid. *Chem. Phys. Lett.* 501: 335–339, 2011.

12) Y. Fujiwara, N. Saito. Ion beam generation from a protic ionic liquid source with an externally wetted tungsten needle. *J. Appl. Phys.* 126: 244901, 2019.

13) Y. Fujiwara. Electrochemical reactions of ionic liquid in vacuum and their influence on ion-beam production by electrospray. *J. Electrochem. Soc.* 167: 166504, 2020.

14) M. Zabet-Moghaddam, R. Krüger, E. Heinzle, A. Tholey. Matrix-assisted laser desorption/ionization mass spectrometry for the characterization of ionic liquids and the analysis of amino acids, peptides and proteins in ionic liquids. *J. Mass Spectrom.* 39: 1494–1505, 2004.

15) J. H. Gross. Liquid injection field desorption/ionization-mass spectrometry of ionic liquids. *J. Am. Soc. Mass Spectrom.* 18: 2254–2262, 2007.

16) L. C. Chen, M. M. Rahman, K. Hiraoka. Non-vacuum field desorption ion source implemented under super-atmospheric pressure. *J. Mass Spectrom.* 47: 1083–1089, 2012.

17) J. H. Gross. Desorption of positive and negative ions from activated field emitters at atmospheric pressure. *Eur. J. Mass Spectrom.* 29: 21–32, 2023.

18) J. H. Gross. Desorption of positive and negative ions from areoles of *Opuntia microdasys* cactus at atmospheric pressure: Cactus-MS. *Mass Spectrom. (Tokyo)* 13: A0146, 2024.

19) Z. B. Alfassi, R. E. Huie, B. L. Milman, P. Neta. Electrospray ionization mass spectrometry of ionic liquids and determination of their solubility in water. *Anal. Bioanal. Chem.* 377: 159–164, 2003.

20) G. P. Jackson, D. C. Duckworth. Electrospray mass spectrometry of undiluted ionic liquids. *Chem. Commun.* 2004: 522–523, 2004.

21) P. J. Dyson, I. Khalaila, S. Luettgen, J. S. McIndoe, D. Zhao. Direct probe electrospray (and nanospray) ionization mass spectrometry of neat ionic liquids. *Chem. Commun.* 2004: 2204–2205, 2004.

22) L. C. Chen, M. K. Mandal, K. Hiraoka. High pressure (>1 atm) electrospray ionization mass spectrometry. *J. Am. Soc. Mass Spectrom.* 22: 539–544, 2011.

23) L. C. Chen, M. K. Mandal, K. Hiraoka. Super-atmospheric pressure electrospray ion source: Applied to aqueous solution. *J. Am. Soc. Mass Spectrom.* 22: 2108–2114, 2011.

24) L. C. Chen, S. Ninomiya, K. Hiraoka. Super-atmospheric pressure ionization mass spectrometry and its application to ultrafast online protein digestion analysis. *J. Mass Spectrom.* 51: 396–411, 2016.

25) Z. Han, L. C. Chen. Generation of ions from aqueous Taylor cones near the minimum flow rate: "True nanoelectrospray" without narrow capillary. *J. Am. Soc. Mass Spectrom.* 33: 491–498, 2022.

26) Z. Han, L. C. Chen. A subtle change in nanoflow rate alters the ionization response as revealed by scanning voltage ESI-MS. *Anal. Chem.* 94: 16015–16022, 2022.

27) Z. Han, N. Omata, T. Matsuda, S. Hishida, S. Takiguchi, R. Komori, R. Suzuki, L. C. Chen. Tuning oxidative modification by a strong electric field using nanoESI of highly conductive solutions near the minimum flow rate. *Chem. Sci.* 14: 4506–4515, 2023.

28) Z. Han, S. Hishida, N. Omata, T. Matsuda, R. Komori, L. C. Chen. Feedback control of electrospray with and without an external liquid pump using the spray current and the apex angle of a Taylor cone for ESI-MS. *Anal. Chem.* 95: 10744–10751, 2023.

29) G. Taylor. Disintegration of water drops in an electric field. *Proc. R. Soc. Lond. A* 280: 383–397, 1964.

30) J. Fernández De La Mora, I. G. Loscertales. The current emitted by highly conducting Taylor cones. *J. Fluid Mech*. 260: 155–184, 1994.

31) A. M. Gañán-Calvo. The surface charge in electrospraying: Its nature and its universal scaling laws. *J. Aerosol Sci*. 30: 863–872, 1999.

32) H. Metwally, Q. Duez, L. Konermann. Chain ejection model for electrospray ionization of unfolded proteins: Evidence from atomistic simulations and ion mobility spectrometry. *Anal. Chem*. 90: 10069–10077, 2018.

33) J. L. Stephenson Jr., S. A. McLuckey. Counting basic sites in oligopeptides via gas-phase ion chemistry. *Anal. Chem*. 69: 281–285, 1997.

34) T. G. Flick, S. I. Merenbloom, E. R. Williams. A simple and robust method for determining the number of basic sites in peptides and proteins using electrospray ionization mass spectrometry. *Anal. Chem*. 83: 2210–2214, 2011.